Journal of Materials Chemistry A

Accepted Manuscript

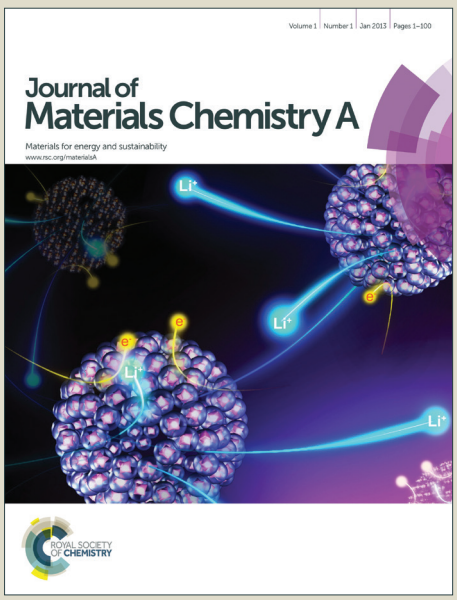

ROYAL SOCIETY OF CHEMISTRY

www.rsc.org/materialsA

Cite this: DOI: 10.1039/c0xx00000x

www.rsc.org/xxxxxx

ARTICLE TYPE

Zn-Al layered double oxides as a high-performance anode materials for zinc-based secondary battery

Jianhang Huang,[a,b] Zhanhong Yang,*[a] Ruijuan Wang,[a,b] Zheng Zhang,[a,b] Zhaobin Feng,[a,b] and Xiaoe Xie[a,b]

Received (in XXX, XXX) Xth XXXXXXXXX 20XX, Accepted Xth XXXXXXXXX 20XX
DOI: 10.1039/b000000x

In this work, Zn-Al layered double oxides (Zn-Al-LDO) was prepared via a facile hydrothermal method followed by calcination treatment in atmosphere of air and evaluated for anode materials of Zn/Ni batteries. The morphology and structure of as-prepared Zn-Al-LDO and the precursor Zn-Al layered double hydroxides (Zn-Al LDH) are investigated through Fourier transform infrared spectra (FT-IR), X-ray diffraction (XRD), scanning electron microscopy (SEM) and Transmission Electron Microscopy (TEM). Compared to Zn-Al-LDH precursor, Zn-Al-LDO possesses higher discharge capacity, better reversibility and longer cycle life, the discharge capacity of Zn-Al-LDO remains about 460 mAh g^{-1} after 1000 cycles. Specially, a good rate performance can be observed for Zn-Al-LDO electrode. The superior properties could be ascribe to the improved charge conductivity and the absence of carbonate anion which make the migration of hydroxyl anion smooth to meet require of electrochemical reaction of electrode.

Introduction

In recent years, there is an overwhelming need for a reliable, stable and cost effective energy storage device for applications ranging from large-scale energy storage to electric and hybrid vehicle applications. As so far, the favorite battery system in the market is lead-acid battery and Li-ion battery. The ability to supply high surge current, along with their low cost, makes lead-acid battery widely used in motor vehicles to provide high current required by automobile starter motors. But it also brings serious polluting to the environment which does not meet the requirements of environment protection. As to lithium ion battery, although it has high energy densities among rechargeable batteries[1, 2], the safety problems due to flammability put constrains to various energy storage applications[3, 4]. Moreover, its insufficient power density due to the limited Li^+ ion conductivity in aprotic electrolytes, and the high cost limit the application field of Li ion battery[5, 6]. On the other hand, the most used zinc electrode in the field of primary battery possesses advantages of low equivalent weight, reversibility, high specific energy density, abundance and low toxicity, and is the most electropositive metal that is relatively stable in aqueous and alkaline media without significant corrosion[7-11]. Recently, startup Imprint Energy is developing flexible, zinc-based rechargeable batteries that can be printed cheaply on commonly used industrial screen printers, which is meant to make the batteries safe for on-body applications. Lithium-based batteries are highly reactive and have to be protected in ways that add size, bulk as well as costing, while zinc is more stable, which allows zinc-based batteries cheap to manufacture, and small size and flexibility of batteries could be realized. Such advantages make the zinc-based batteries become a very attractive and promising battery system.

However, a fundamental problem will arise when used as anode material for secondary batteries, it is so called "dendrite formation", which mainly derive from a high solubility of zinc active material in alkaline electrolyte[12, 13]. The discharge products such as zincate ions dissolved out into electrolyte during electric discharge exhibit non-uniform deposition onto electrodes at the time of charging process, resulting in a dendritic formation[14-16]. This dendrite would cause increase of polarization, the loss in discharge capacities and, at worst, the internal short-circuit when the dendrites grow up to the opposite positive electrode[17]. Many efforts have been made to mitigate or suppress dendrite formation, most of researchers have focused on the electrolyte, modification of ZnO and additives in the electrodes[9, 18]. A large variety of inorganic additives, such as Ca(II)[19, 20], Bi(III)[21-23], In(III)[24-26], Ba(II)[27], were added into zinc electrodes, and found that they can suppress the dendrite formation of zinc electrode to different extent. In addition, organic additives, such as surfactants with pi electrons of fused rings[28], polyaniline and polypyrrole[29, 30], were also adopted to stable the zinc electrode. Furthermore, the effects of different size and morphology on electrochemical performances of ZnO electrodes were widely investigated,[31, 32] it was found that the growth mode of as-prepared ZnO nanoparticles has changed due to intensive extension effect, and suppressed the production of ZnO dendrite and enhanced capacity maintenance. With proper approach, the stability of zinc electrode can be greatly improved. S.C.P.S. developed a zinc electrode modified with titanium nitride. As an ceramic conductor, titanium nitride helps to retain zincate ions, allowing a uniform zinc deposition on charge. This electrode is capable of more than 800 cycles without obvious degradation.[33] J. Phillips et al.[34]

developed a Nickel-Zinc battery for high rate applications, in which the zinc electrode was modified with silica and fluoride (reduces zinc solubility and mobility). This cell can achieve 1000 cycles at high current rate although there is 60% capacity fade.

However, few investigations have been devoted to the alternative active material. In our previous works[35], hydrotalcite and its modified materials have been proposed as novel zinc electrode materials and the electrochemical properties were studied in details. The results show that hydrotalcite evaluated as anodic materials for Zn/Ni batteries exhibit better electrochemical cycling stability compared with conventional ZnO. But the theory capacity of hydrotalcite is low because of its larger molecular weight. Therefore, it is need to explore new anodic materials with a larger specific capacity as well as superior electrochemical performance. In recent years, calcination products of LDHs which known as layered double oxides (LDO) have been paid more attention owing to their larger surface area and less diffusion resistance than that of LDHs[36]. In this work, zinc-based layered double oxide was prepared and evaluated as anode material for alkaline electrolyte secondary cell. It shows satisfying capacity retention which is about 460 mAh g^{-1} after 1000 cycles.

Experimental section

Preparation of Zn-Al layered double oxides nanocomposites

The Zn-Al-hydrotalcities (Zn-Al-LDH) were prepared by a hydrothermal method. In typical synthesis, an aqueous solution (100 ml) of Zn and Al nitrates (Zn: Al molar ratio equal to 3:1) with total metal ion concentration of 0.25 mol L^{-1} was added into batch reactor containing 50 ml of distilled water, keep the flow rate at 5 ml min^{-1}. Meanwhile, an alkaline solution (100 mL) of Na_2CO_3 (0.0125 mol) and NaOH (0.05 mol) was simultaneously added into above batch reactor in order to retain the pH value at 10. The synthesis process was carried out under vigorous stirring at 45 °C, then transferred the above reaction solution to a reaction kettle with continually stirring for 10 min, then sealed the kettle and kept it in thermostatic drying closet, reacting at 120 °C for ten hours. Filtering, washing and then vacuum drying at 60 °C over night. As to obtain the Zn-Al layered double oxides nanocomposites (Zn-Al-LDO), the as-synthesized Zn-Al-LDH powders were calcined in atmosphere of air at 600 °C for 6h. The product of Zn-Al-LDO were collected and packed in a PE bag for further examination and use.

Characterization of Zn-Al-LDO samples

Thermogravimetry-Differential scanning calorimetry (TG-DSC) analysis was conducted on NET ZSCH STA 449C. Fourier transform infrared spectra (FT-IR) of the samples were conducted on a Nicolet Nexus-670 FT-IR spectrometer (as KBr discs, with wave number 400−4000 cm^{-1}, and the weight of measured sample is 2 mg). XRD patterns of samples were recorded by a D500 (Siemens) diffractometer (36 kV, 30 mA) using Cu Kα radiation at a scanning rate of 2θ=8° min^{-1}. The morphology of the Zn-Al-LDO products was examined by SEM (JSM-6360LV) and TEM (JEM-2100F). The specific surface areas of the samples were analyzed by Brunauer–Emmett–Teller (BET) nitrogen adsorption–desorption measurement (Quantachrome Instrument, NOVA2000e).

Preparation and electrochemical measurements of the Zn-Al-LDO electrodes

The Zn-Al-LDO electrodes were prepared by incorporation of slurries of 85 wt. % Zn-Al-LDO, 10 wt. % acetylene black and 5 wt. % additives of polytetrafluoroethylene (PTFE, 60 wt. %, in diluted emulsion). Copper mesh (1.0 cm×1.0 cm in size) was served as the current collector and the Zn-Al-LDO electrodes were roll-pressed to a thickness of 0.2 mm. Then, the obtained Zn-Al-LDO electrodes were dried at 60 °C under vacuum. For comparison, Zn-Al-LDH electrodes composed of Zn-Al-LDH were also fabricated by the same way. The positive electrode was the commercial sintered $Ni(OH)_2$ electrode (Tianjin City Fine Chemical Research Institute) whose capacity was much larger than Zn-Al-LDO electrode for making full use of the active material in Zn-Al-LDO electrode. The electrolyte is solution of 6 M KOH saturated with ZnO. All the cells were pre-activated for 10 times by the following operations: The cells were charged at constant current of 1C for 60 min, and discharged at constant current of 1C to a cut-off voltage of 1.2 V.

A three-electrode cell was assembled for cyclic voltammograms (CV) and electrochemical Impedance Spectroscopy (EIS), with Hg/HgO electrode served as the reference electrode, pre-activated pasted zinc electrode as the working electrode and the sintered Nickel electrode as counter electrode. CV was carried out on an electrochemical workstation (CHI660D) at room temperature at a scanning rate of 5 mV·s^{-1} range from -0.8 V to -1.8 V. EIS analysis were carried out using an Parstat 2273 (Princeton Applied Research) electrochemical workstation over the frequency range from 100 kHz to 0.1 Hz, the amplitude of the AC potential perturbation was 10 mV. And EIS data was fitted using the software of Zview. The galvanostatic charge-discharge tests were performed on a BTS-5V/10mA battery-testing instrument (Neware, China) at room temperature.

In all the above experiments, the reagents used were A.R. grade and the electrolyte was prepared with deionized water.

Results and discussions

TG-DSC analysis was conducted in order to obtain an appropriate conversion temperature from the precursor to Zn-Al-LDO. As

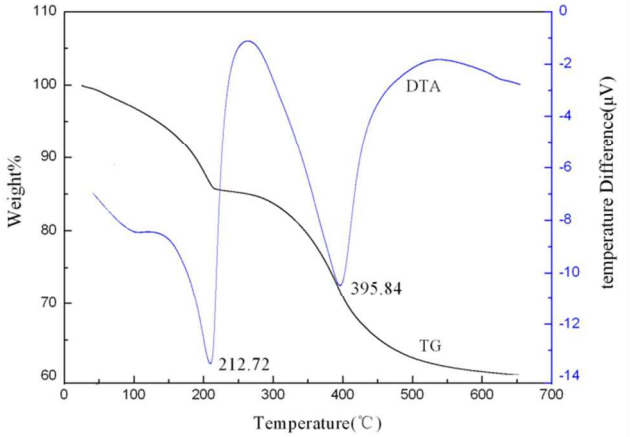

Fig. 1 TG-DSC curves of Zn-Al-LDH samples from 100 to 700 °C at a heating rate of 10 °C min^{-1} under atmosphere

shown in Fig. 1, the weight loss of the precursor mainly happens before 600°C. Around the 100 °C there is a relative week endothermic peak, which could be ascribed to the elimination of absorbed water. Furthermore, there is an intense endothermic peak around 212 °C, which corresponds to the weight loss for the second stage of weight loss. It is probably due to the elimination of interlayer water in the LDHs flakes, which can be expressed as following reaction equation:

$$[Zn_6Al_2(OH)_{16}](CO_3)\cdot mH_2O=[Zn_6Al_2(OH)_{16}](CO_3)+mH_2O \quad (1)$$

Afterwards, the third stage between 212 and 500 °C is mainly attributed to the decomposition of OH^- in LDHs layers and the accompanied decomposition of CO_3^{2-} in the interlayer spaces, which can be described as follow equation:

$$[Zn_6Al_2(OH)_{16}](CO_3)=6ZnO+Al_2O_3+CO_2+8H_2O \quad (2)$$

The related TG-DSC results of as-prepared LDH samples are in good agreement with those previous works reporting for Zn-Al-LDH samples [37]. So in order to make sure the complete conversion from LDH to LDO, the reaction temperature for Zn-Al-LDH was set at 600 °C.

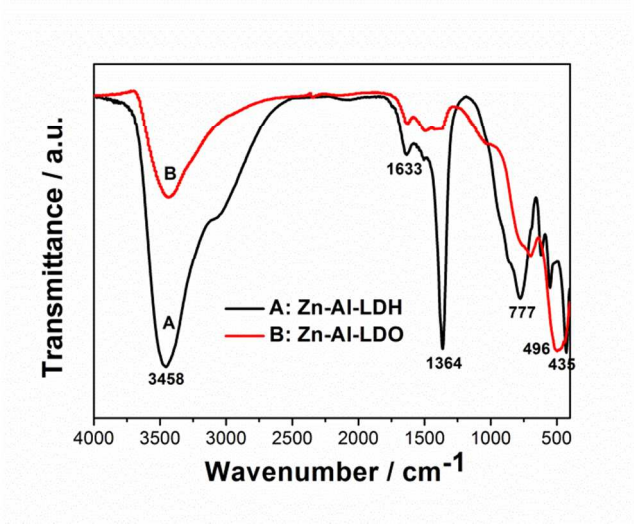

Fig.2 FT-IR spectra of Zn-Al-LDH (curve A) and Zn-Al-LDO (curve B)

FT-IR spectra of Zn-Al-LDO and Zn-Al-LDH between 4000–400 cm−1 wavenumber are shown in Fig. 2 in order to investigate the situation of anionic functional groups between interlayer. As to Zn-Al-LDH sample (curve A), it displays absorption band at 3458 cm^{-1} owing to the O–H stretching and flexural oscillations of OH^- group. Based on the crystal structure of LDH, each OH^- group in the LDH layer is bonded to three metal cations[36]. Therefore, the superposition of bands belonging to $3Zn^{2+}$– OH, $2Zn^{2+}Al^{3+}$– OH, $Zn^{2+}2Al^{3+}$– OH and $2Al^{3+}$– OH resulted in the broad band at 3000–3750 cm^{-1}. But as to Zn-Al-LDO sample (curve B), the absorption band around 3458 cm^{-1} is obviously weaker than that of LDH, indicating that it was only caused by the absorbed water introduced during testing process, but no OH^- group in the cationic interlayer.

Furthermore, the significant absorption bands at 1633 and 1364 cm^{-1} for Zn-Al-LDH can be assigned to C−O asymmetric stretching because of the existence of carbonate in Zn-Al-LDH. However, from curve B we can see that the corresponding absorption peak of C−O asymmetric stretching for Zn-Al-LDO is much weaker, illustrating that most of carbonate has been eliminated after calcination under 600 °C.

In addition, there are some absorption peaks appearing between 400 and 800 cm^{-1} for both of Zn-Al-LDH and Zn-Al-LDO samples, and they can be considered as the lattice vibrations for Zn-O and Al-O. Because of the absence of carbonate and hydroxyl, the locations of absorption peaks assigned to Zn-O and Al-O exhibit some shift compared to Zn-Al-LDH.

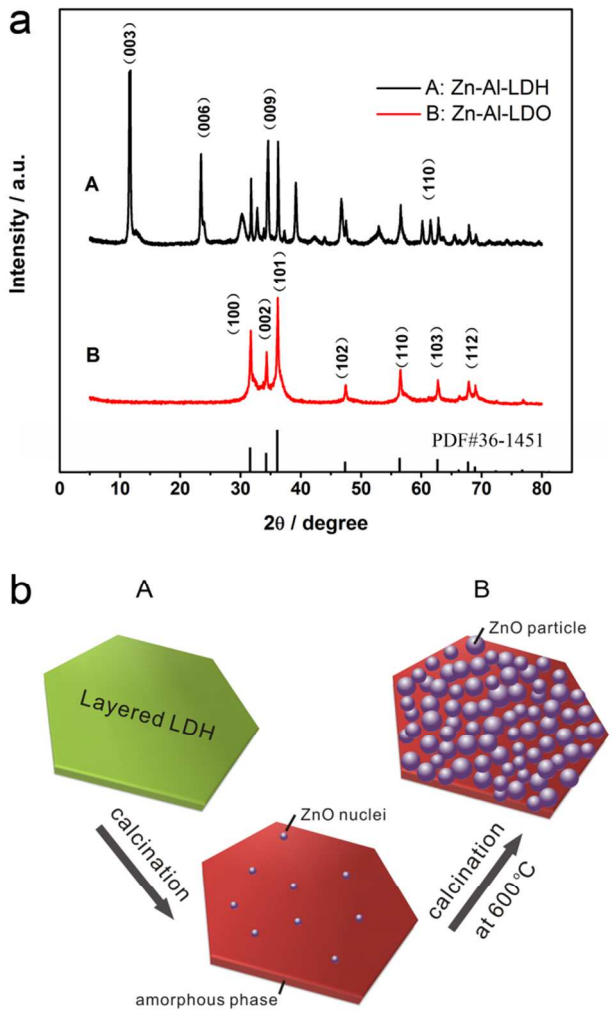

Fig. 3 (a) XRD patterns of Zn-Al-LDH (curve A) and Zn-Al-LDO (curve B) (b) Schematic diagram of the transformation from LDH to LDO

Fig. 3a gives the comparison of XRD patterns of the precursor Zn-Al-LDH (curve A) and Zn-Al-LDO (curve B) nanosheets respectively. It can be seen from curve A that the LDH precursor displays the characteristic XRD patterns of a layered hydrotalcite-like material, in which the characteristic diffraction peaks of LDH at 2θ = 11.71º, 23.55º, 34.64º and 60.20º corresponding to (003), (006), (009) and (110) planes of layered hydrotalcite-like material can be observed, respectively. As to the Zn-Al-LDO derived from calcinations of LDH precursor at 600 °C, its XRD pattern is agree well with the typical ZnO phase of the hexagonal wurtzite structure (JSPDS No.36-1451). There is no diffraction peak of aluminum oxide observed in curve B. The absence of diffraction peak of aluminium species

could be associated with the mechanism of the transformation of LDH precursor to LDO, which have reported in previous study[38]: during the calcination process, Zn-Al-LDH precursor first transfer into ZnO nuclei doped with Al^{3+} which exist as amorphous phase, then the increasing temperature lead to the preferred orientation of ZnO along the (101) direction and the two-dimensional expansion of ZnO phase in sheet-like structure. The schematic diagram of the transformation from LDH to LDO is provided in Fig. 3b.

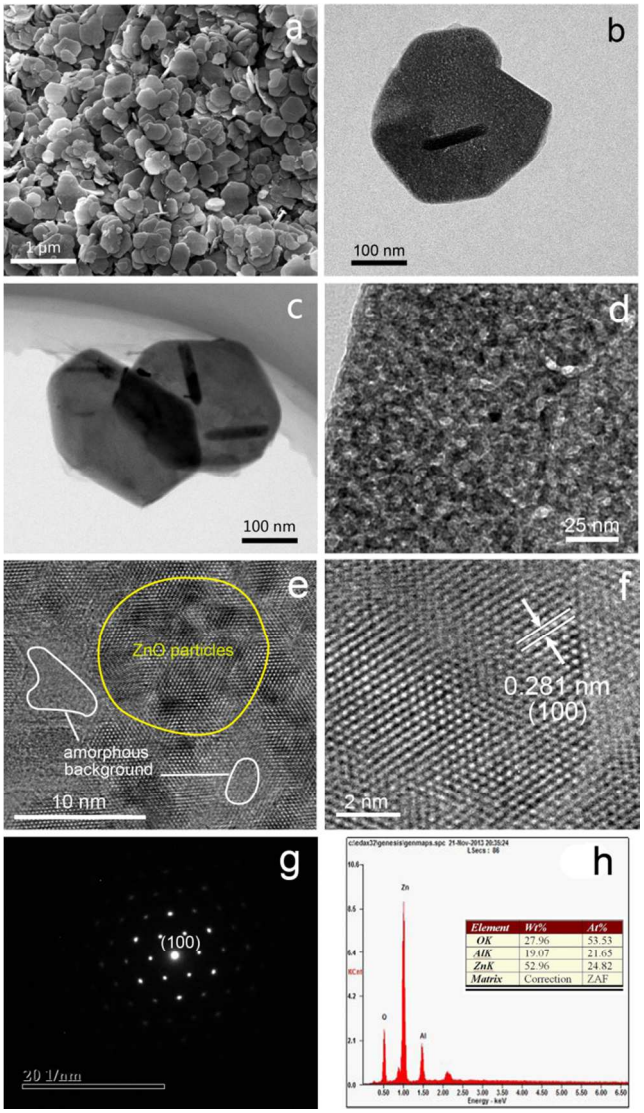

Fig. 4 (a) SEM image of as-prepared LDO sample; (b,c) TEM images of as-prepared LDO and LDH; (d,e) Magnified TEM image of LDO; (f) HRTEM image of LDO; (g) Electron diffraction patterns of LDO; (h) EDS result from Zn-Al-LDO nanosheets

The morphology and microstructure of the as-prepared Zn-Al-LDO was characterized by SEM and TEM. From Fig. 4a we can see that the Zn-Al-LDO sample typically consists of uniform and thin hexagonal nanosheets, which is consistent with the sheet-like morphology of Zn-Al-LDH, it is the typical structure of the 2D material, and the particle size of Zn-Al-LDO nanosheets is about 200-400 nm. The further detailed structure information about Zn-Al-LDO nanosheets could be observed in TEM images which shown in Fig 4b. As can be seen that although the sheet-like morphology of LDH precursor has been maintained, the roughness of the surface becomes more serious compared with that of LDH which is given in Fig 4c. Fig 4d gives the magnified image of sheet-like Zn-Al-LDO, the ZnO nanoparticles (dark field) uniformly embedded in the amorphous matrix (bright field), forming the sheet-like morphology. These results are agreement with that of XRD pattern why there is only diffraction peak of ZnO observed. The further magnified image is given in Fig. 4e in order to further understand the construction of LDO sample. As can be seen in Fig. 4e that one of dark field highlighted with yellow contours possesses obvious and clear lattice fringes, while some bright field highlighted with white contours shows no lattice fringes. The observations enable us clearly distinguish zinc oxide particles from the amorphous background. Fig. 4f shows the clear lattice fringes in the HRTEM image of LDO, the distances between the adjacent lattice planes are 0.281 nm, corresponding to the (100) planes of ZnO, which is consistent with the SAED result shown in Fig. 4g, and the selected electron diffraction pattern has a typical six-fold symmetry, confirming that the sample is of high-quality single crystal nature. In addition, EDS spectrum measurement (Fig. 4h) confirmed the presence of Zn and Al in Zn-Al-LDO. The specific surface areas of LDH and LDO estimated with the BET method are 30.8 and 32.9 m^2g^{-1}, respectively. A little larger specific surface areas of LDO is associated with the rough surface.

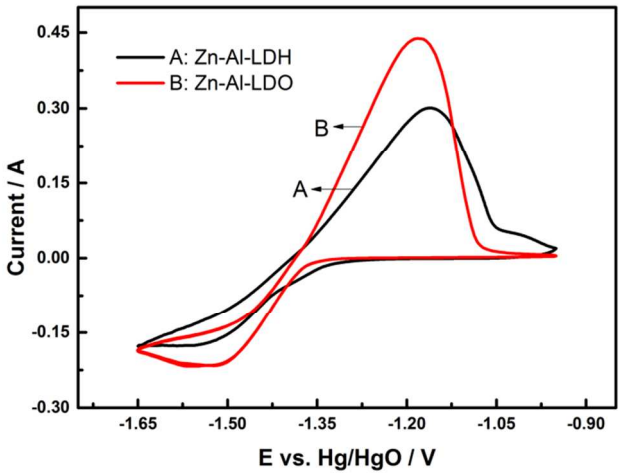

Fig. 5 Cyclic voltammograms for zinc electrodes with Zn-Al-LDH (curve A) and Zn-Al-LDO (curve B)

In order to investigate the electrochemical performance of Zn-Al-LDO, cyclic voltammetry analysis were carried out and the comparison of cyclic voltammetry curves of Zn-Al-LDH (curve A) and Zn-Al-LDO (curve B) are shown in Fig. 5. As can be seen that LDO electrode shows lower anodic peak potential, larger anodic peak area, and the anode peak is much steeper compared with that of LDH electrode. Generally, the anodic process is corresponding to the discharge process of secondary battery. These characteristics of anode peak mentioned above indicate that LDO possess rapid oxidizing reaction kinetics, and the discharging process is more effective. That is to say, LDO possess the higher electrochemical activity, and can deliver higher discharge capacity than that of LDH. Furthermore, the anodic peak of Zn-Al-LDH and Zn-Al-LDO can be observed at –

1.160 V and –1.182 V, respectively, and the corresponding cathodic peaks for LDH and LDO appears at -1.537 V and -1.529 V, respectively. So the potential interval between anodic peak and cathodic peak can be obtained, which is taken as a measurement of the reversibility of electrode reaction: the smaller the potential interval is, the better the reversibility will be. From Fig. 5, it can be calculated that the potential interval of LDH and LDO is 0.377V and 0.347V, respectively. Indicating LDO electrode possess better reversibility than that of LDH. The improved electrochemical properties could be attributed to the structure of Zn-Al-LDO which has got rid of interlayer CO_3^{2-}.

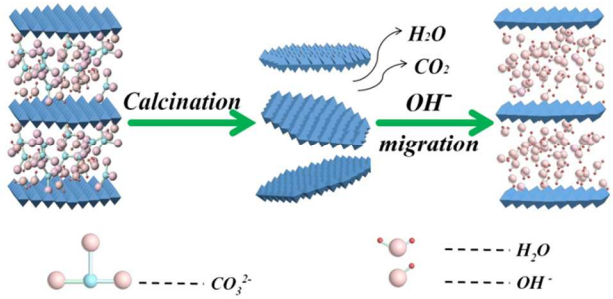

Fig. 6 Schematic of the elimination of CO_3^{2-} and the migration of OH^-

The absence of CO_3^{2-} can facilitate the migration of hydroxyl aions between layers of LDO and then make sure that the electrochemical reaction will proceed smoothly. The schematic plot of this process is shown in Fig. 6. This result could also be verified by the phenomenon of two anodic peaks of LDH. There is a small shoulder peak appearing around –1.0 V for LDH, but there is no similar peak observed as to LDO. The two anodic peaks correspond to two processes of anodic dissolution, which can be explained by the oxidation reaction of Zn, according to following equations:

$$Zn + 4OH^- \leftrightarrow Zn(OH)_4^{2-} + 2e^- \quad (3)$$

$$Zn + 3OH^- \leftrightarrow Zn(OH)^{3-} + 2e^- \quad (4)$$

Reaction (3) corresponds to the first anodic peak at –1.160 V, which occurs when the amount of hydroxyl anion in electrolyte is adequate. It has been proceeding for some time at a lower over-potential, leading to an exhaust of hydroxyl anions between interlayers of LDH. And the existence of carbonates hinders the diffusion of hydroxyl anions into the bulk of solid LDH, finally results in an inadequate supply of hydroxyl anion. So equation (4) will perform and the second peak appears around –1.0 V.

EIS measurements are performed to analyze the difference of charge transfer resistance between Zn-Al-LDH and Zn-Al-LDO. Fig. 7a shows the nyquist plots of the Zn-Al-LDO electrode and Zn-Al-LDH electrode. It can be seen that both the nyquist plots of LDH and LDO include a semicircles in the region of high frequency and a slope tail in the low frequency. Generally speaking, the diameter of semicircle represents the charge-transfer resistance (R_{ct}), and the slope in the low frequency region is caused by the semi-infinite diffusion. In addition, the equivalent circuit for the electrode is shown in Fig. 7b, where *CPE* designates the constant-phase element. R_e is the total ohmic resistance which includes the resistance of the electrolyte, current collector, etc. R_{ct} is the charge-transfer resistance and Z_w is the Warburg impedance. Distinctly, after calcinations, the charge transfer resistance of LDO electrode is reduced greatly.

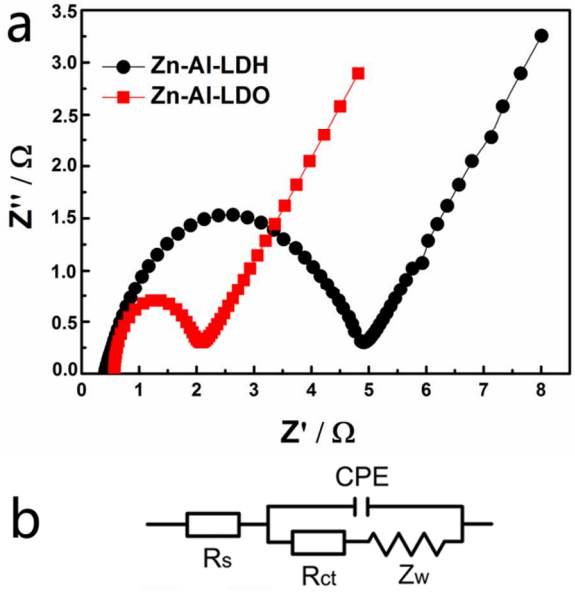

Fig. 7 (a) Nyquist plots of the electrodes with Zn-Al-LDH and Zn-Al-LDO at 100% state-of-charging and (b) equivalent circuit for the electrode

According to the equivalent circuit, the R_{ct} of Zn-Al-LDO and Zn-Al-LDH can be calculated as 1.49 Ω cm^2 and 4.57 Ω cm^2, respectively. The lower R_{ct} imply the improvement of electronic conductivity of the LDO anode. It is conductive to the fast transport of electron in the active material and leads to a good reversibility of electrode. As we know that in the Zn-Al-LDH structure, zinc hydroxide octahedra doped with Al ion share edges to form brucite-like layer with positive charge which is balanced by anions arranged in interlayer galleries. So there is no free electron in LDH, resulting in the poor conductivity, and the conductivity of Zn-Al-LDH is lower than 10^{-5} S cm^{-1} measured in our previous work[18]. But after calcination, LDH transform into LDO containing ZnO species. As a semiconductor, the conductivity of ZnO is about 10^{-2} S cm^{-1},[39] which is much better than LDH. So the improvement of conductivity is caused by the formation of ZnO phase and the uniform distribution of ZnO particles in LDO after calcination, the conductivity of which is much better than that of LDH with CO_3^{2-} between the interlayer.

The cycling stability is evaluated with Zn-Al-LDH and Zn-Al-LDO as anode materials, and the assembled Zn/Ni batteries were charged and discharged at current density of 1C, and the cycle performances of electrodes were shown in Fig. 8. Zn-Al-LDH shows regular cycling performance, it is relative stable in the first 300 cycles and then gradually decline in the discharge capacity during subsequent charge-discharge cycles. The reversible discharge capacity of LDH electrode at first 300 cycles is average 374mAh g^{-1}, revealing 93%retention. However, there is only 163 mAh g^{-1} maintained after 800 cycles, the retention rate of discharge capacity drop rapidly to 41%. As to Zn-Al-LDO, the higher average discharge capacity of 469 mAh g^{-1} discharge capacity can be observed, and it is relative stable, it can be observed that there is 460 mAh g^{-1} remained after 1000 cycles with a high retention of 96%. The improved cycle performance of Zn-Al-LDO is attributed to the improved conductivity and the

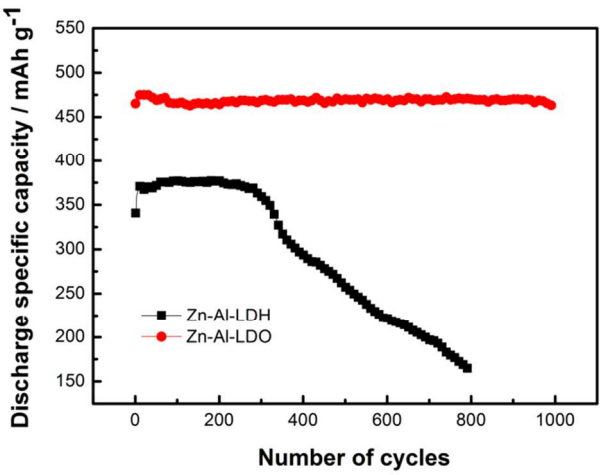

Fig. 8 Cycling performance of Zn-Al-LDH (curve A) and Zn-Al-LDO (curve B)

increased percentage of zinc species in electrode, which leads to smaller polarization and more even distribution of current than that of Zn-Al-LDH electrode, finally slow down the decomposition of electrode. The improved properties can also be observed from the comparison of charge/discharge curves between Zn-Al-LDH and Zn-Al-LDO electrode. The galvanostatic charge/discharge curves of Zn/Ni batteries using the Zn-Al-LDH and Zn-Al-LDO electrodes at the 50th cycle are displayed in Fig. 9. As we can see in Fig. 9 that Zn-Al-LDO anode show lower charge plateau voltage as well as higher discharge plateau voltage compared to Zn-Al-LDH anode, the potential difference between the charging and discharging curve of Zn-Al-LDO electrode is smaller than that of Zn-Al-LDH electrode, this indicates that the reversibility of LDO electrode is improved compared to Zn-Al-LDH electrode. Not only because the ZnO phase in LDO possess better conductivity than LDH, but also the absence of CO_3^{2-} provide a unblocked passageway for migration of OH^- which guarantees the smooth progress of the electrode reaction. Furthermore, it is worth noting that the

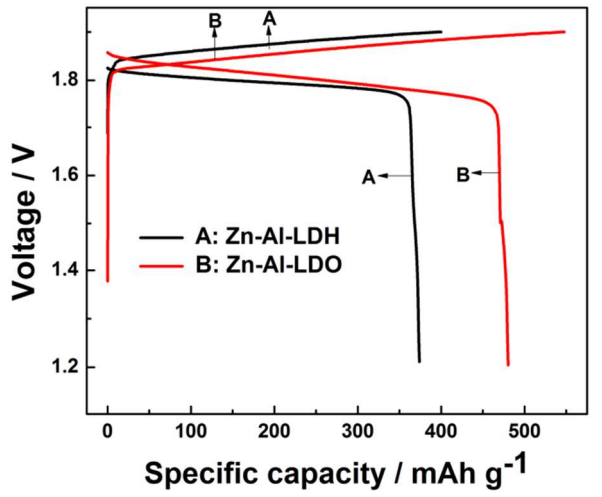

Fig. 9 Typical galvanostatic charge-discharge curves of Nickel-Zinc secondary batteries with Zn-Al-LDH (curve A) and Zn-Al-LDO electrode (curve B) at 50th cycle

discharge specific capacity of Zn-Al-LDO is ~90 mAh g^{-1} higher than that of Zn-Al-LDH. The absence of CO_3^{2-} in the Zn-Al-LDO can be considered as the main reason for the increased specific capacity. As we know, CO_3^{2-} is interlayer anions located in the interlayer space of LDH for charge compensation, so it has no contribution to discharge capacity of electrode. When the LDH has been converted to LDO with calcination treatment, CO_3^{2-} was

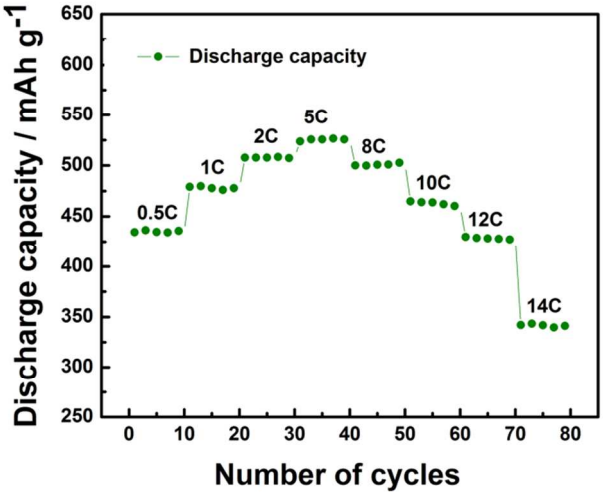

Fig. 10 Rate capability of Zn-Al-LDO

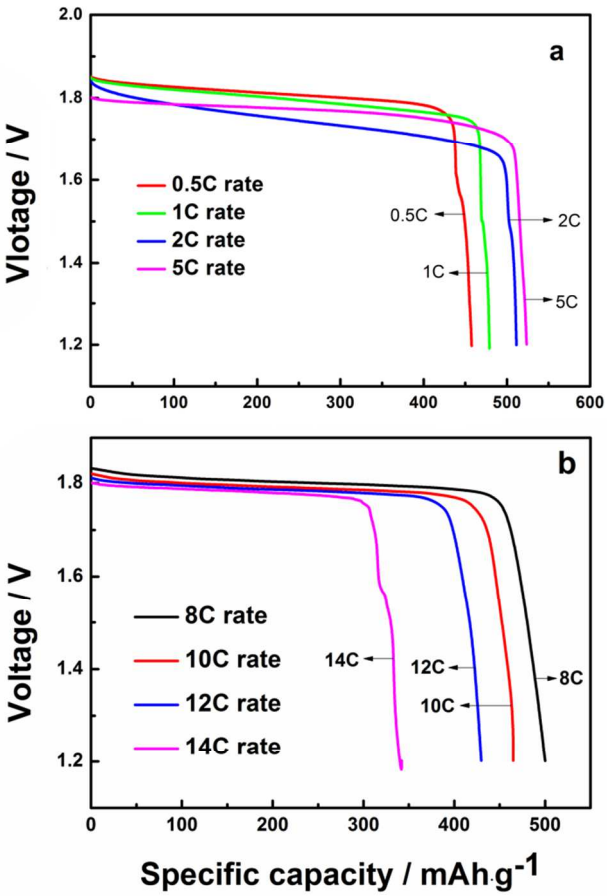

Fig. 11 The discharge curves of Zn-Al-LDO electrodes at various current densities from 0.5C to 14C rate

dislodged, and the percentage of ZnO was enhanced in LDO, therefore, the specific capacity of Zn-Al-LDO electrodes accordingly increased.

Rate performance is an important evaluation factor for measuring the performance of zinc electrode in meeting the needs of high-storage applications. In order to study the rate performance of Zn-Al-LDO, the assembled Zn/Ni batteries were charged/discharged at different current rates between 1.2V and 1.9V, respectively. An interesting rate performance of Zn-Al-LDO electrode can be observed in Fig. 10, the discharge capacity keeps increase with the increasing discharge rate until that the discharge rate reaches 5C. When the discharge rate continues to increase, the Zn-Al-LDO electrode presents a gradual decrease in discharge capacity. Furthermore, Fig. 11 shows the corresponding discharge curves of the Zn-Al-LDO at various current densities. As we can see that the Zn-Al-LDO electrode exhibits discharge capacity of 453 mAh g^{-1}, 476 mAh g^{-1}, 508 mAh g^{-1} and 518 mAh g^{-1} at the current of 0.5C, 1C, 2C rate and 5C rate, respectively. However, the discharge capability declined when the current rate keep increasing after 5C, and it exhibits the discharge capacity of 500 mAh g^{-1}, 464.9 mAh g^{-1}, 429.8 mAh g^{-1} and 342.1 mAh g^{-1}, respectively.

When the current rate was lower than 5C, the increase of discharge capacity with increasing current rate can be ascribed to the enhanced charge efficiency of zinc electrode which is caused by the improvement in suppression of hydrogen evolution when they are cycled at the high rate. The Tafel empirical formula about evolution of hydrogen is described as following:

$$\eta_{H2} = a + b \log j \qquad (5)$$

Where η_{H2} represents the hydrogen evolution over-potential, a is the constant value related to electrode materials, b is constant value of 0.116 V, and j represents current density. It is obvious that the hydrogen evolution over-potential is in direct proportion to the electric current density. In other words, with the increase of charge rate during the high-rate charge process, the hydrogen evolution over-potential will be enhanced, which is beneficial to restrain the evolution of hydrogen during charge process. Although the increasing current rate makes the polarization of Zn-Al-LDO electrode more and more serious simultaneously (the increasing polarization of testing electrode could be noticed in the charge curves in Fig. 11, the discharge plateau decrease with increase of current rate), the inhibit effect on evolution of hydrogen plays the dominant role when the current rate is lower than 5C, so the charge efficiency will be improved, and then the according discharge capacity could be enhanced. Furthermore, the discharge capacity decrease gradually when the current rate continues to increase after 5C. It because that when the increasing charge rate is during a high rate region (higher than 5C), the aggravation of electrode polarization becomes the most important role in the charge/discharge process of electrodes, and the inhibition of hydrogen evolution could be ignored. The high polarization leads to the significant decline in charge/discharge efficiency, finally weakens the discharge capacity of Zn-Al-LDO.

Conclusions

Layered Zn-Al layered double oxide was prepared through hydrothermal method, followed by a calcinations treatment which in order to eliminate the carbonate. As-prepared LDO samples exhibit layered morphology with particle size of 200-400 nm, it was consisted of hexagonal wurtzite ZnO doped with Al^{3+} which exist as amorphous phase. High discharge capacity and long cycle was observed when LDO was evaluated as anode material for Zn/Ni secondary battery, the improved performance benefited from the layered structure and high active material content with enhanced conductivity caused by elimination of carbonate. These results provide important insights for develop new anode materials for promising Zinc-based secondary batteries.

Acknowledgement

We are grateful for financial support from the Natural Science Foundation of China (No. 21371180), Doctoral Fund of Ministry of Education of China (20130162110 018) and the Science and Technology Project of Changsha city (No. k1303015-11).

Notes and references

[a] *College of Chemistry and Chemical Engineering, Central South University, Changsha 410083, Chin. E-mail: jhhuangcsu320@gmail.com*
[b] *Innovation base of energy and chemical materials for graduate students t raining, Central South University, Changsha 410083, China.*

1. Y. Li and H. Dai, *Chemical Society reviews*, 2014, **43**, 5257-5275.
2. V. Aravindan, J. Gnanaraj, Y.-S. Lee and S. Madhavi, *Journal of Materials Chemistry A*, 2013, **1**, 3518-3539.
3. X. Zhou, L. J. Wan and Y. G. Guo, *Advanced Materials*, 2013, **25**, 2152-2157.
4. P. Poizot, S. Laruelle, S. Grugeon, L. Dupont and J. Tarascon, *Nature*, 2000, **407**, 496-499.
5. K. Xu, *Chemical reviews*, 2004, **104**, 4303-4418.
6. M. Gong, Y. Li, H. Zhang, B. Zhang, W. Zhou, J. Feng, H. Wang, Y. Liang, Z. Fan, J. Liu and H. Dai, *Energy & Environmental Science*, 2014, **7**, 2025-2032.
7. J. Huang, Z. Yang, B. Yang, R. Wang and T. Wang, *Journal of Power Sources*, 2014, **271**, 143-151.
8. J. Huang, Z. Yang and T. Wang, *Electrochimica Acta*, 2014, **123**, 278-284.
9. J. Jiri, *Journal of Power Sources*, 1997, **66**, 15-25.
10. J. Jiri, *Journal of Power Sources*, 2000, **88**, 202-205.
11. Z. Feng, Z. Yang, J. Huang, X. Xie and Z. Zhang, *Journal of Power Sources*, 2015, **276**, 162-169.
12. A. P. Pavlov, L. K. Grigorieva, S. P. Chizhik and V. K. Stankov, *Journal of Power Sources*, 1996, **62**, 113-116.
13. T. Wang, Z. Yang, B. Yang, R. Wang and J. Huang, *Journal of Power Sources*, 2014, **257**, 174-180.
14. J. Diggle, A. Despic and J. M. Bockris, *Journal of The Electrochemical Society*, 1969, **116**, 1503-1514.
15. B. Yang, Z. Yang and R. Wang, *Journal of Power Sources*, 2014, **251**, 14-19.
16. X. Xie, Z. Yang, Z. Feng, Z. Zhang and J. Huang, *Electrochimica Acta*, 2015, **154**, 308-314.
17. K. Miyazaki, Y. S. Lee, T. Fukutsuka and T. Abe, *Electrochemistry*, 2012, **80**, 725-727.
18. B. Yang, Z. Yang, R. Wang and Z. Feng, *Journal of Materials Chemistry A*, 2014, **2**, 785-791.
19. Y. F. Yuan, J. P. Tu, H. M. Wu, Y. Li, D. Q. Shi and X. B. Zhao, *Journal of Power Sources*, 2006, **159**, 357-360.
20. R. Wang, Z. Yang, B. Yang, X. Fan and T. Wang, *Journal of Power Sources*, 2014, **246**, 313-321.
21. J. McBreen and E. Gannon, *Journal of Power Sources*, 1985, **15**, 169-177.
22. Y. F. Yuan, Y. Li, S. Tao, F. C. Ye, J. L. Yang, S. Y. Guo and J. P. Tu, *Electrochimica Acta*, 2009, **54**, 6617-6621.
23. Y. F. Yuan, L. Q. Yu, H. M. Wu, J. L. Yang, Y. B. Chen, S. Y. Guo and J. P. Tu, *Electrochimica Acta*, 2011, **56**, 4378-4383.

24. S. Wang, Z. Yang and L. Zeng, *Journal of the Electrochemical Society*, 2009, **156**, A18-A21.
25. R. Wang, Z. Yang, B. Yang, T. Wang and Z. Chu, *Journal of Power Sources*, 2014, **251**, 344-350.
26. X. Fan, Z. Yang, W. Long, Z. Zhao and B. Yang, *Electrochimica Acta*, 2013, **92**, 365-370.
27. Y. Zheng, J. Wang, H. Chen, J. Zhang and C. Cao, *Materials chemistry and physics*, 2004, **84**, 99-106.
28. R. K. Ghavami and Z. Rafiei, *Journal of Power Sources*, 2006, **162**, 893-899.
29. J. Vatsalarani, S. Geetha, D. C. Trivedi and P. C. Warrier, *Journal of Power Sources*, 2006, **158**, 1484-1489.
30. J. Vatsalarani, D. C. Trivedi, K. Ragavendran and P. C. Warrier, *Journal of The Electrochemical Society*, 2005, **152**, A1974-A1978.
31. Y. F. Yuan, J. P. Tu, H. M. Wu, Y. Li and D. Q. Shi, *Nanotechnology*, 2005, **16**, 803-808.
32. R. Wen, Z. Yang, X. Fan, Z. Tan and B. Yang, *Electrochimica Acta*, 2012, **83**, 376-382.
33. G. l. Toussaint, P. Stevens, L. Akrour, R. Rouget and F. Fourgeot, 2010, 25-34.
34. J. Phillips, S. Mohanta, M. Geng, J. Baron, B. McKinney and J. Wu, *ECS Transactions*, 2009, **16**, 11-17.
35. X. Fan, Z. Yang, R. Wen, B. Yang and W. Long, *Journal of Power Sources*, 2013, **224**, 80-85.
36. W. Shi, M. Wei, L. Jin and C. Li, *Journal of Molecular Catalysis B: Enzymatic*, 2007, **47**, 58-65.
37. N. D. Didier Tichit, Bernard Coq, and Robert Durand, *Chem. Mater*, 2002, **14**, 1530-1538.
38. X. Zhao, F. Zhang, S. Xu, D. G. Evans and X. Duan, *Chemistry of Materials*, 2010, **22**, 3933-3942.
39. B. Hong Youl and C. Gyeong Man, *Sensors and Actuators B*, 1999, 47-54.

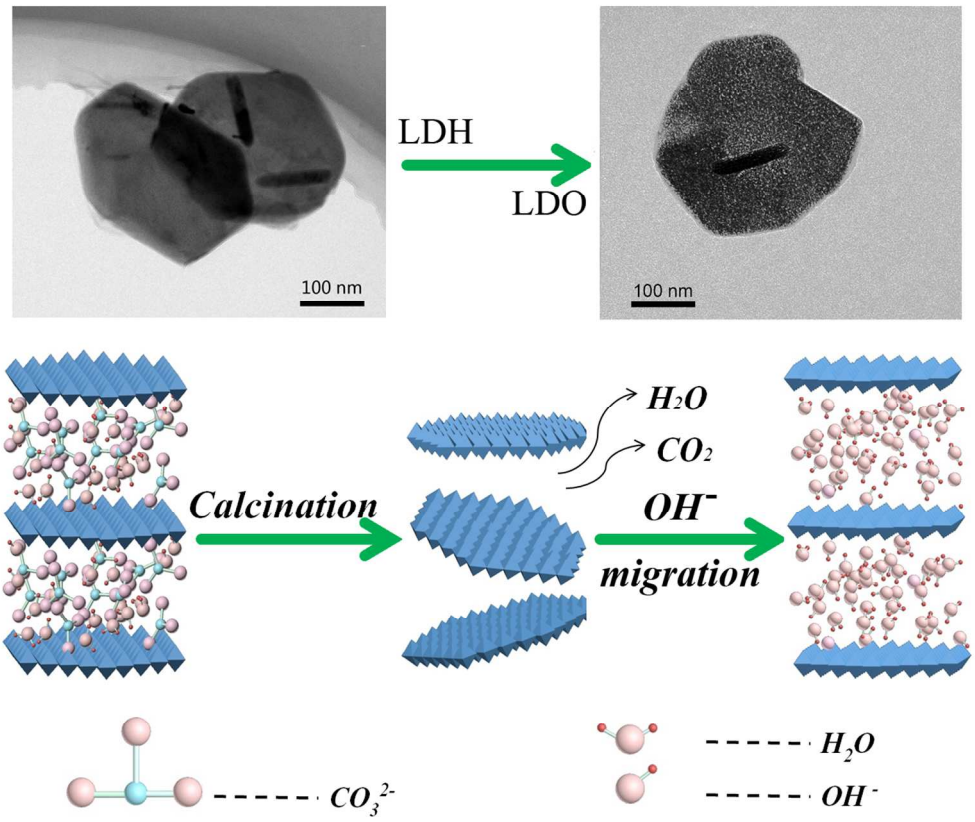

Graphical Abstract
115x97mm (300 x 300 DPI)